Nanoscale

PAPER

View Article Online
View Journal | View Issue

Cite this: *Nanoscale*, 2024, **16**, 18882

Nanorod-associated plasmonic circular dichroism monitors the handedness and composition of α-synuclein fibrils from Parkinson's disease models and post-mortem brain†

Francesca Longhena, [a,b] Rihab Boujebene,[a] Viviana Brembati,[a] Michele Sandre,[c] Luigi Bubacco,[c] Sergio Abbate, [a,d] Giovanna Longhi *‡[a,d] and Arianna Bellucci *‡[a]

Human full-length (fl) αSyn fibrils, key neuropathological hallmarks of Parkinson's disease (PD), generate intense optical activity corresponding to the surface plasmon resonance of interacting gold nanorods. Herein, we analysed fibril-enriched protein extracts from mouse and human brain samples as well as from SK-N-SH cell lines with or without human fl and C-terminally truncated (Ctt) αSyn overexpression and exposed them to αSyn monomers, recombinant fl αSyn fibrils or Ctt αSyn fibrils. *In vitro*-generated human recombinant fl and Ctt αSyn fibrils and fibrils purified from SK-N-SH cells with fl or Ctt αSyn overexpression were also analysed using transmission electron microscopy (TEM) to gain insights into the nanorod-fibril complexes. We found that under the same experimental conditions, bisignate circular dichroism (CD) spectra of Ctt αSyn fibrils exhibited a blue-wavelength shift compared to that of fl αSyn fibrils. TEM results supported that this could be attributed to the different properties of nanorods. In our experimental conditions, fibril-enriched PD brain extract broadened the longitudinal surface plasmonic band with a bisignate CD couplet centred corresponding to the absorption band maximum. Plasmonic CD (PCD) couplets of *in vivo*- and *in vitro*-generated fibrils displayed sign reversal, suggesting their opposite handedness. Moreover, the incubation of *in vitro*-generated human recombinant fl αSyn fibrils in mouse brain extracts from αSyn null mice resulted in PCD couplet inversion, indicating that the biological environment may shape the handedness of αSyn fibrils. These findings support that nanorod-based PCD can provide useful information on the composition and features of αSyn fibrils from biological materials.

Received 19th July 2024,
Accepted 9th September 2024

DOI: 10.1039/d4nr03002h

rsc.li/nanoscale

Introduction

Under genetic and/or environmental pathological conditions, intrinsically disordered proteins may misfold and form toxic fibrillar deposits that are the major cause of a wide range of neurodegenerative disorders.[1] Among them, Parkinson's disease (PD) is currently the second most common neurodegenerative disorder after Alzheimer's disease. The presence of Lewy bodies (LBs), which are pathological proteinaceous inclusions mainly composed of α-synuclein (αSyn) fibrils, is among the key neuropathological hallmarks of PD together with nigrostriatal neuron degeneration.[2–4] Notably, although full-length (fl) αSyn fibrils are most abundant at the periphery of LBs, the cores of these inclusions contain substantial amounts of C-terminally truncated (Ctt) αSyn.[5–7] This fact supports the hypothesis that Ctt αSyn plays a critical role in initiating fibrillary aggregation, which in line with evidence supporting that different Ctt forms of αSyn have been found to display improved aggregation potential.[6,8,9] Ctt fibrils also exhibit improved prion-like ability to induce the formation of endogenous fl αSyn aggregates in recipient cells,[8] suggesting that their aggregation-seeding activity may significantly contribute to pathology diffusion. Furthermore, Ctt αSyn fibrils exhibit distinctive features such as a tighter packed core and improved proteinase K resistance compared to fl αSyn fibrils,[10] supporting that they may be distinguished from fl fibrils using biophysical methods with easy and quick accessibility.

[a]*Department of molecular and Translational Medicine, University of Brescia, Viale Europa 11, 25123 Brescia, Italy. E-mail: arianna.bellucci@unibs.it, giovanna.longhi@unibs.it*
[b]*Department of Clinical Neurosciences-Clifford Allbutt Building, University of Cambridge, Hills Road CB2 0AH, Cambridge, UK*
[c]*Department of Biology, University of Padova, Via Ugo Bassi 58b, 35121 Padua, Italy*
[d]*Istituto Nazionale di Ottica, INO-CNR, Research Unit of Brescia, c/o CSMT, Via Branze 35, 25123 Brescia, Italy*

†Electronic supplementary information (ESI) available. See DOI: https://doi.org/10.1039/d4nr03002h

‡These authors contributed equally.

Chiroptical spectroscopy has been often used to monitor fibril formation. In particular, circular dichroism (CD) in the far UV region has been widely applied to detect changes in the secondary structure of proteins undergoing fibrillation. In the case of αSyn, this technique has been helpful to confirm the content of large β-sheets.[11,12] Moreover, Raman optical activity (ROA) gave information on αSyn in solution,[13,14] while vibrational circular dichroism (VCD)[14] and infrared (IR) spectroscopy were also used to monitor the secondary structure and the fibrillation process of fl and Ctt αSyn in the presence of β-synuclein.[15,16]

Chiroptical spectroscopy studies suggest that fibrils can grow with a specific chirality (namely right- or left-handed), depending on the external physico-chemical conditions, such as pH and temperature. Indeed, induced CD (iCD) signals of opposite sign have been obtained from thioflavin T (ThT) and Congo red (CR) bound to insulin fibrils grown under different temperature conditions.[17,18] Opposite circularly polarized luminescence (CPL) was also detected from ThT interacting with fibrils of opposite chirality.[19] Interestingly, even induced lanthanide CPL has been found to be quite sensitive to fibrillation.[20] Finally, VCD is sensitive to the fibril morphology,[21] and it has been recently used to follow the handedness of winding for a 12-residue αSyn fragment with putative aggregation-triggering capacity.[22]

In the last decade, the use of plasmonic nanoparticles has generated great interest due to their ability to bind *via* both covalent and non-covalent interactions different biological molecules such as DNA, peptides and thiol group-containing biomolecules. When nanoparticles are embedded in chiral templates such as biomolecules, plasmonic chirality takes place, giving rise to a CD response.[23–28] Furthermore, nanoparticles with a controlled size, shape, composition and distinctive physicochemical and electrical properties can be designed[24] and this has opened unprecedented opportunities for the discovery of biomarkers and therapeutics.[29,30]

In this line, it has been recently shown that nanorod-shaped particles form helical arrangements upon non-covalent interactions with fl αSyn fibrils, resulting in intense optical activity at the longitudinal surface plasmon resonance (LSPR) wavelength.[31,32] This technique has enabled the detection of fibrils from post-mortem PD brains as well as infectious amyloid formed by prion proteins down to nanomolar concentrations.[31]

Herein, we aimed to assess the nanorod-based plasmonic CD (PCD) spectra of αSyn fibrils of different biological origin, investigating the possibility of distinguishing fl- and Ctt-generated fibrils and comparing the signal obtained from *in vitro*-generated pre-formed fibrils (PFF) with that derived from *in vivo*-formed fibrils. For this purpose, we tested and compared different biological samples with two batches of commercial gold nanorods of slightly different dimensions, and thus with corresponding different wavelengths of the plasmonic bands. Employing these nanorods, we analysed the PCD spectra of the fibrils isolated from the brains of mice injected with adeno-associated viral (AAV) vectors inducing human fl αSyn overexpression in the nigrostriatal system (AAV-hαSyn)[33,34] and human Ctt (1–120 aa) αSyn transgenic (Syn120 tg) mice,[35–37] two different models of PD exhibiting the presence of αSyn fibrils. Subsequently, we analysed fibril-enriched extracts from the post-mortem brain of a PD patient and an age-matched control and synthetic human fl and Ctt (1–120 aa) αSyn PFF and fibrils isolated from different lines of human neuroblastoma SK-N-SH cells overexpressing human fl or Ctt αSyn and exposed to either human fl or Ctt αSyn PFF or fl or Ctt αSyn monomers. The interaction of nanorods with either fl or Ctt αSyn PFF was also analysed by transmission electron microscopy (TEM). Finally, we checked whether the PCD response of insulin fibrils can be employed to follow the changes in fibril morphology, given that the insulin fibril model may provide key insight for understanding nanorod-assembly handedness.

Materials and methods

Animals

C57BL/6J wild-type (wt) mice, human C-terminally truncated (1–120 aa) αSyn transgenic (Syn120 tg) mice[35–37] and mice carrying a spontaneous deletion of αSyn locus SNCA[38] (Null) (C57BL6/JOlaHsd, Harlan) were used for this study. The mice were bred in our animal house facility at the Department of Molecular and Translational Medicine of University of Brescia, Brescia, Italy. The animals were maintained under a 12 h light–dark cycle at room temperature (RT) of 22 °C and had *ad libitum* access to food and water. All experiments were carried out in accordance with Directive 2010/63/EU of the European Parliament and of the Council of 22 September 2010 on the protection of animals used. All experimental procedures conformed to the National Research Guide for the Care and Use of Laboratory Animals and were approved by the Animal Research Committees of the University of Brescia (Protocol Permit 719/2015-PR). All efforts were made to minimize animal suffering and reduce the number of mice used.

Animal surgery

Two-month-old (25 g) C57BL/6J wt mice were bilaterally injected in the substantia nigra with AAV serotype 2/6 inducing the overexpression of human αSyn (5×10^{13} genome copies per mL, AAV-hαSyn), as described in.[33] Briefly, the animals were anesthetized and placed in a stereotactic head frame (Stoelting, IL, USA). After making a midline incision in their scalp and drilling a hole in the appropriate location for the substantia nigra at the left and the right site of the skull, 2 μL of viral vector was injected at a rate of 0.2 μL min^{-1} with a 33-gauge needle on a 10 μL Hamilton syringe at the following coordinates: antero-posterior − 3.60; medio-lateral + 1.15; dorsal–ventral − 3.75 relative to Bregma. The needle was left in place for an additional 5 min before being slowly retracted from the brain. The mice were sacrificed at 8 weeks from the AAV injections for the extraction of αSyn fibrils.

Human tissues

Caudate putamen fresh frozen tissue from one patient with PD (PD45, male 80 yo, 19 years of disease duration) and one age-matched control subject (PDC029, male 82 yo), kindly supplied by the Parkinson's UK Brain Bank, a Charity funded by Parkinson's UK (Imperial College London, UK), were used for the extraction of αSyn fibrils. The study on the human brain samples was performed in accordance with the local clinical research regulations and obtained approval from the Ethics Committee of Brescia District.

Sucrose gradient extraction of αSyn fibrils

The separation of αSyn aggregates due to a sucrose gradient allows the extraction of αSyn high-order aggregates and fibrils from tissues and/or cells.[39,40] Briefly, the cells and tissues were homogenized in 9 vol (wt/vol) of ice-cold membrane signal extraction (MSE) buffer [10 mM MOPS/KOH, pH 7.4, 1 M sucrose, 1 mM ethylene glycol-bis(b-aminoethyl ether)-*N*,*N*,*N*0, *N*0-tetraacetic acid (EGTA) and 1 mM EDTA with proteasome inhibitor mixture (Roche Diagnostics)]. For the purification of αSyn fibrils, a sucrose step gradient was prepared by overlaying 2.2 M with 1.4 M, and finally with 1.2 M sucrose in volume ratios of 1 : 2 : 2 (vol/vol). The homogenate was layered on the gradient and centrifuged at 160 000*g* for 3 h using a SW40 rotor (Beckman Coulter). Twelve fractions of 1 mL were collected from each gradient from top (fraction 1) to bottom (fraction 12) and analysed for the presence of αSyn fibrils by adding a nanorod solution, identifying the ones with CD signal.

Nanorods

Two types of commercial gold nanorods were used, including nanorods with a diameter of 10 nm and length of 30 nm and nanorods with a diameter of 10 nm and length of 25 nm with LSPR peaks at 695 nm and 640 nm, respectively. They were purchased from Nanopartz, Loveland, Co, U.S.A., and used as received, that is, stock solutions of 1.59 nM and 2.13 nM concentration in 18MEG DI water, capped with cetyltrimethylammonium bromide (CTAB) to prevent their spontaneous aggregation, 5 mM and 3 mM was the CTAB concentration in the two batches, respectively. The capped rods had a positive zeta potential of +33 mV and +35 mV, respectively, and the solution pH varied in the range pH of 6–7.

Treatment of SK-N-SH neuroblastoma cell line with αSyn fibrils

Human neuroblastoma SK-N-SH cells and SK-N-SH cells stably overexpressing fl αSyn or truncated Ctt (1–120) αSyn were grown in complete medium comprised of Dulbecco's modified Eagle's medium (DMEM) with 1000 mg glucose per L (Sigma Aldrich) supplemented with 10% heat-inactivated fetal bovine serum, 100 μg mL^{-1} penicillin, 100 μg mL^{-1} streptomycin and 0.01 μM non-essential amino acids (Sigma-Aldrich). The cells were maintained at 37 °C under a humidified atmosphere of 5% CO_2 and 95% O_2. For αSyn PFF treatment, the cells were seeded on 6 cm Ø dishes (80 000 cells per dish) and maintained in growth medium. The αSyn monomers and PFF were diluted at 100 nM final concentration in growth medium, and then sonicated 10 times, 10 s each time with 50% power with a SonoPlus HD 2070. After that, the cell medium was replaced with monomer/PFF-containing medium. The cells were incubated with monomer/fibril medium, and after 72 h the cells were collected with PBS for sucrose gradient extraction of the αSyn fibrils.

Extraction from HEK cells

HEK cells were grown in a medium comprised of DMEM with 4500 mg glucose per L supplemented with 10% heat-inactivated fetal bovine serum, 100 μg mL^{-1} penicillin, 100 μg mL^{-1} streptomycin and 0.01 μM non-essential amino acids. The cells were maintained at 37 °C under a humidified atmosphere of 5% CO_2. For sucrose gradient purification, the cells were seeded on 6 cm Ø dishes (80 000 cells per dish) and maintained in growth medium until they reached 80–90% confluence, and then collected with PBS.

Formation of nanorod-αSyn fibril complexes and CD measurements

Several tests were carried out to choose the most appropriate buffer for forming the nanorod-fibril complex to obtain the best CD signal, *i.e.*, by considering the intensity and symmetry of the observed couplet. Water, PBS, Tris HCl and phosphate buffer were assayed at different pH and salt concentrations. The best choice was Tris HCl 25 mM, pH = 8, 150 mM NaCl for the first type of nanorods (10 × 30 nm) and 80 mM NaCl for the second one (10 × 25 nm). The difference in salt content was related to the CTAB concentration. Salt is necessary to remove CTAB and favour the nanorod-fibril interaction. Subsequently, 1 mL buffer was added to 1 mL of purchased nanorod solution. αSyn monomers and PFF fibrils for both fl and Ctt protein were added, as illustrated in the figure captions. For the experiments with biological samples, 100 μL neuroblastoma cell extracts, 100 μL HEK cells, 100 μL mouse brain homogenate extracts or 100 μL sample of human brain homogenates extracts were added to 1 mL nanorod solution and 1 mL of the previously described buffer.

All PCD spectra were recorded with a CD JASCO 815SE machine with 10 accumulations at a resolution of 2 nm, using a 1 cm quartz cuvette. In all the spectroscopic measurements, reporting CD as $\Delta A = A_L - A_R$ (L and R indicate left and right circularly polarized light, respectively), we cannot exclude contributions from chiral scattering components;[41] we checked that linear dichroism is negligible (as expected with a randomly distributed suspension).

Preparation of fl and Ctt (1–120) αSyn PFF

Monomers in fl and Ctt (1–120) form of human αSyn were prepared as previously described,[42] then suspended in phosphate-buffered saline (PBS) at pH = 7.4, and then filtered with a 100K Millipore filter to get rid of residual aggregates caused by lyophilisation. The absorbance of UV radiation from soluble pro-

teins was measured at 280 nm. Then, the protein concentration was calculated using the molar extinction coefficients corresponding to 5960 M^{-1} cm^{-1} and 1490 M^{-1} cm^{-1} for αSyn fl and Ctt (1–120) αSyn, respectively. To obtain fibrils, 0.05% of NaN_3 was added to solubilise proteins at a concentration of 340 μM and the solution was heated at 37 °C under vortexing at 1000 rpm in an Eppendorf Thermomixer for one week. Subsequently, PFF was collected by centrifuging the sample for 15 min at 15 000*g* and by preserving the pellet. The residual soluble αSyn that was present in the supernatant was quantified using the same extinction coefficients by subtracting the initial amount used for aggregation from the soluble protein present in the supernatant to determine the amount of αSyn converted to PFF after the end of the process. Then, the PFF were resuspended in PBS to a final equivalent monomeric concentration of 250 μM and stored at −80 °C.[43] In fact it is known that it is necessary to store the solution with αSyn PFF either at room temperature or at −80 °C because storing it at 4 °C or −20 °C can lead to significant dissociation.[44,45]

Transmission electron microscopy (TEM)

Fl and Ctt (1–120) αSyn PFF were characterized through TEM imaging using negative staining. Fibrils were diluted 1 : 10 in distilled water and placed on a formvar and carbon-coated 200-mesh copper grid (Ted Pella). The sample was directly stained with 2% uranyl acetate. TEM images were acquired on a Tecnai G2 12 Twin instrument (FEI, Hillsboro, OR).

For the nanorod-fibril complex, nanorods with 10 × 30 nm dimensions at 0.5 nM concentration were added to 1.12 μM PFF solutions in Tris buffer, as mentioned above. The solution was incubated at room temperature for 1 h for fibrils generated from fl form and for 2 h for Ctt (1–120) αSyn PFF (the incubation time was decided based on the PCD results) before proceeding with the preparation for TEM analysis as described above. The extraction of fibrils from SK120 and SK140 for TEM imaging was not carried out using sucrose gradient as that for the PCD measurements case. Briefly, the cell pellets were suspended in 10× volume of Tris-buffered saline (TBS)+ solution [50 mM Tris HCl pH 7.4, 175 mM NaCl, 5 mM EDTA, 1 mM *N*-ethylmaleimide, 0.1 mM phenylmethylsulfonyl fluoride (PMSF) and protease inhibitor] and centrifuged for 5 min at 1000*g* at 4 °C. Then, a series of 3 centrifugations using different buffers was carried out for 30 min at 120 000 at 4 °C using an XPN-80 rotor Ty70Ti and the pellet was conserved after each step. The first centrifugation was done using TBS+ followed by another one using 1% Triton/TBS+, and the final centrifugation was done using RIPA buffer [50 mM Tris HCl, 175 mM NaCl, 5 mM EDTA, 0.1 mM PMSF, 0.5 mM sodium deoxycholate, 0.1 mM SDS and NP-40]. The pellet obtained at the end was resuspended in 30 μL Tris buffer. The TEM images of the SK120 and SK140 extracts with nanorods were recorded by adding a 0.5 nM nanorod suspension to a 100 μL volume of cell extracts in 150 μL Tris buffer. The solution was incubated for 1 h before proceeding with the preparation, as described above.

Incubation fl αSyn PFF in αSyn null mouse brain homogenate

Fraction 1 from the sucrose gradient extraction of αSyn null mouse brain homogenate was used to incubate fl αSyn PFF. A final concentration of 3.75 μM of fl αSyn PFF was diluted in fraction 1 and incubated for 24 h at 4 °C. After this, fl αSyn PFF + αSyn null mouse brain homogenate solution was diluted with the nanorod solution and suitable buffer to obtain a final PFF concentration of 375 nM, similar to the experiments with fl and Ctt αSyn PFF alone.

Insulin fibrillation experiments

Insulin monomers were fibrillated *in vitro* following a previously published procedure.[19] Briefly, 1 wt% of bovine insulin purchased from Sigma Aldrich was dissolved in 0.1 M NaCl buffer at pH 1.8. Then 0.6 mL volume of solution was put in a thermomixer under shaking at 1400 rpm for 48 h. To obtain -iCD insulin fibrils (−IF), the temperature in the thermomixer was set at 60 °C, and to obtain +iCD insulin fibrils (+IF), temperature was instead set at 35 °C. Fibrillation and handedness were checked using ThT detecting CD and CPL signal, as previously described.[19]

Formation of nanorod-insulin fibril complex and CD measurements

The set-up experiments showed that the optimal condition to detect the PCD signal from the nanorod-insulin fibril solutions was obtained by the addition of insulin fibrils and 400 mM NaCl to a 2 mL nanorod solution (dimensions 10 × 30 nm) with a final concentration of 1.6 nM for nanorods and 12 μM for + or −insulin fibrils. The spectra were recorded using a CD JASCO 815SE instrument with 5–10 accumulations, using a 1 cm quartz cuvette.

Results and discussion

Detection of fibrils from mouse brain samples

Initially, we examined the PCD spectra of the nanorods with a size of 10 × 30 nm incubated with fibril-enriched protein extracts from AAV-hαSyn, Syn120 tg and αSyn null *substantia nigra* plus *striatum* mouse brain samples to single out the main motifs of the spectra, including their ability to monitor the presence of either fl fibrils or Ctt fibrils (Fig. 1A).

In the first set of experiments, we performed PCD analysis of fibril-enriched protein fractions from the C57BL/6J mice subjected to stereotaxic nigral injections of AAV-hαSyn. In particular, to collect the fibril-enriched protein fractions from freshly dissected mouse brain tissue we used an established protocol of sucrose gradient-based fractionation enabling the separation of proteins based on their relative molecular weight and solubility.[39] The sucrose gradient fractionation-derived protein fractions from the C57BL/6JOlaHsd αSyn null mice, which displayed spontaneous deletion of the αSyn gene locus SNCA,[38] were used as the negative control.

By analysing the 12 fractions obtained from the sucrose gradient-based fractionation of the αSyn null mouse brain

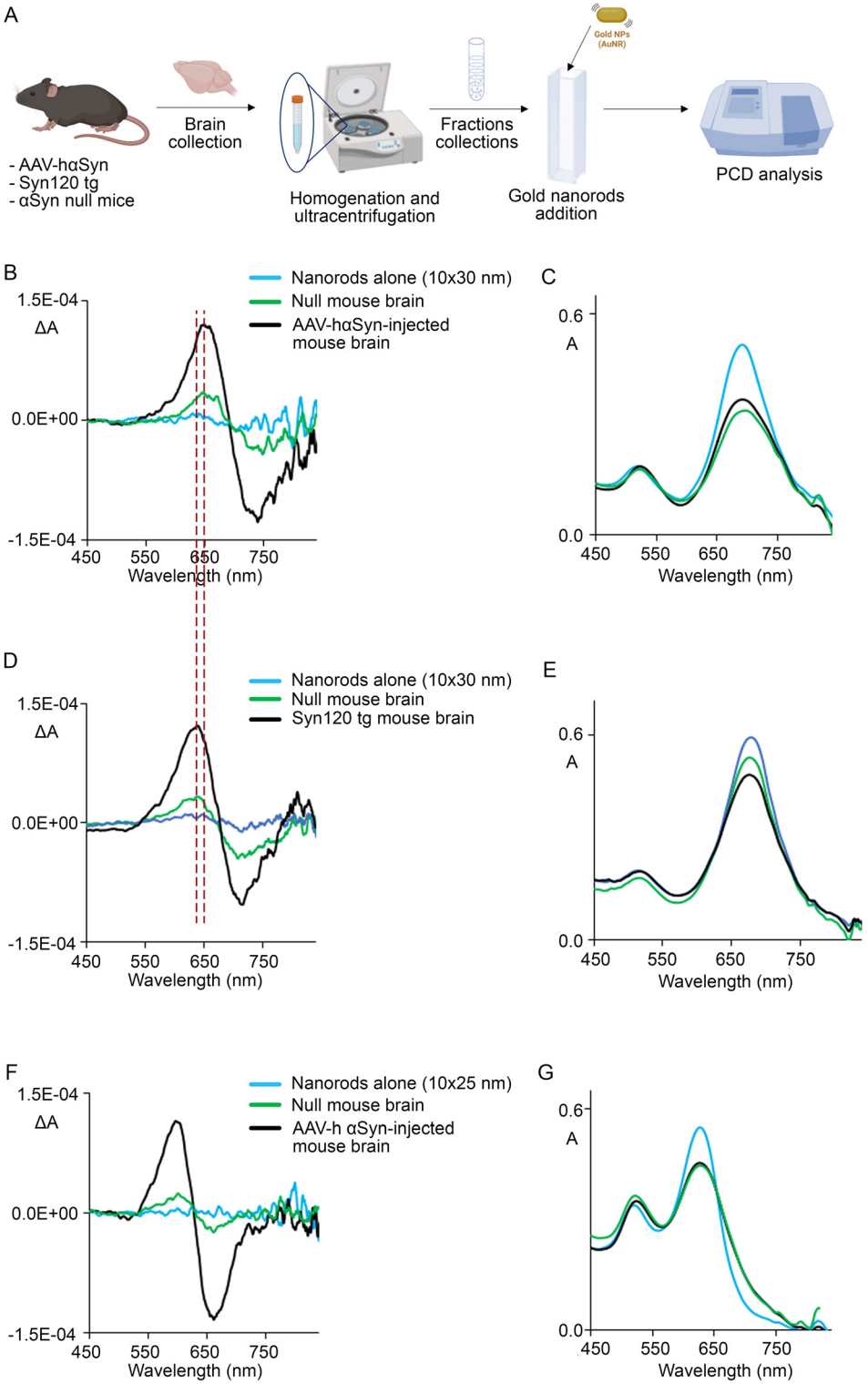

Fig. 1 (A) Schematic representation of the experimental design. (B) CD and (C) absorption spectra of nanorod suspensions (nanorod size: 10 × 30 nm) incubated for 1 h with fractions 4–6 from brain homogenate of AAV serotype injected mice (black line) and fraction 1 of null mice (green line) in comparison with plain nanorod buffer suspension (blue line). (D) CD and (E) absorption spectra of nanorod suspensions (nanorod size: 10 × 30 nm) incubated for 1 h with fractions 4–6 from brain homogenate of 18 months old αSyn120 tg mice (black line) and fraction 1 of null mice (green line) in comparison with plain nanorods buffer suspension (blue line). (F) CD and (G) absorption spectra of nanorod suspensions (nanorod size: 10 × 25 nm) incubated for 1 h with purified AAV mouse brain homogenate (black line) and fraction 1 of null mice (green line) in comparison with plain nanorods buffer suspension (blue line). The two vertical red dotted lines indicate the wavelength position of the positive peaks observed for αSyn120 tg brain samples (lower wavelength) and for AAV-injected brain samples (higher wavelength value). In all the figures: A represents absorbance or optical density and $\Delta A = A_L - A_R$ (L and R indicate left and right circularly polarized light). However, some scattering components and some chiral scattering may be present. Other authors use the term "extinction".

samples with added nanorods, we detected a very weak CD signal from fraction 1, which was interpreted as the presence of some impurity (Fig. 1B, green line). No CD response was obtained for up to 4 h of incubation with all the other fractions, an observation likely supporting the absence or paucity of fibrils in these samples. When we tested the fractions from the nigrostriatal brain samples of AAV-h αSyn-injected mice with the nanorod suspension, we detected a CD signal from fractions 4–6, which correspond to a range of approximately 35% to 75% sucrose. These fractions, considering recent findings,[46] should contain large αSyn species. The addition of 100 μL of optically active fractions to the suspension of nanorods gave a bisignate CD signal (Fig. 1B and C). In particular, the (−,+) couplet was found to be centred in Correspondence of the absorption maximum, which showed a decrease in intensity and broadening compared to the control samples containing only nanorods (Fig. 1B and C).

Subsequently, we analysed fractions 4–6 from the mixed nigral and striatal samples of 18 months old Syn120 tg mice (Fig. 1D and E), where the positive peak was found to display a slight wavelength blue shift compared to the signal obtained from the AAV-h αSyn-injected brains.

By using a second batch of nanorods with a size of 10 × 25 nm, we confirmed the detection of a PCD signal from AAV-hαSyn fibril-enriched brain fractions 4–6 and absence of a reliable signal from the αSyn null mice (Fig. 1F and G). In this case, the CD couplet was far from the spectroscopic range limit accessible to our instrument, an observation that enabled us to exclude the presence of other CD components at a higher wavelength.

Overall, these findings support that gold nanorod-based PCD analysis enables the detection of the presence of αSyn fibrils in mouse brain through very specific CD responses.

Detection of fibrils from *caudate putamen* samples from PD and control brains

To confirm that we could properly detect αSyn fibrils from biological samples, we tested the protein fractions derived from the fibril-enriched sucrose gradient fractions from frozen human post-mortem *caudate putamen* samples of a PD patient with a disease duration of 19 years and a healthy control subject (Fig. 2A), as described by Kumar and co-authors.[31] Following the addition of 100 μL of fibril-enriched fractions 4–6 to the nanorod suspension, we observed that the absorption spectrum exhibited a broadening of the longitudinal surface plasmonic band and the appearance of a bisignated CD couplet centred corresponding to the absorption band maximum, exhibiting the main positive peak at the wavelength of approximately 650 nm (Fig. 2B and C). Interestingly, this wavelength matched that of the peak observed following the nanorod-based PCD analysis of the fibril-enriched extracts from the AAV-hαSyn-injected mice. The presence of a weak signal from healthy patients, which was previously reported also by Kumar,[31] could be due to the fact that a healthy aged human brain may present fibrillary protein accumulation even without disease manifestations.[47] These findings corroborated that we could properly detect the

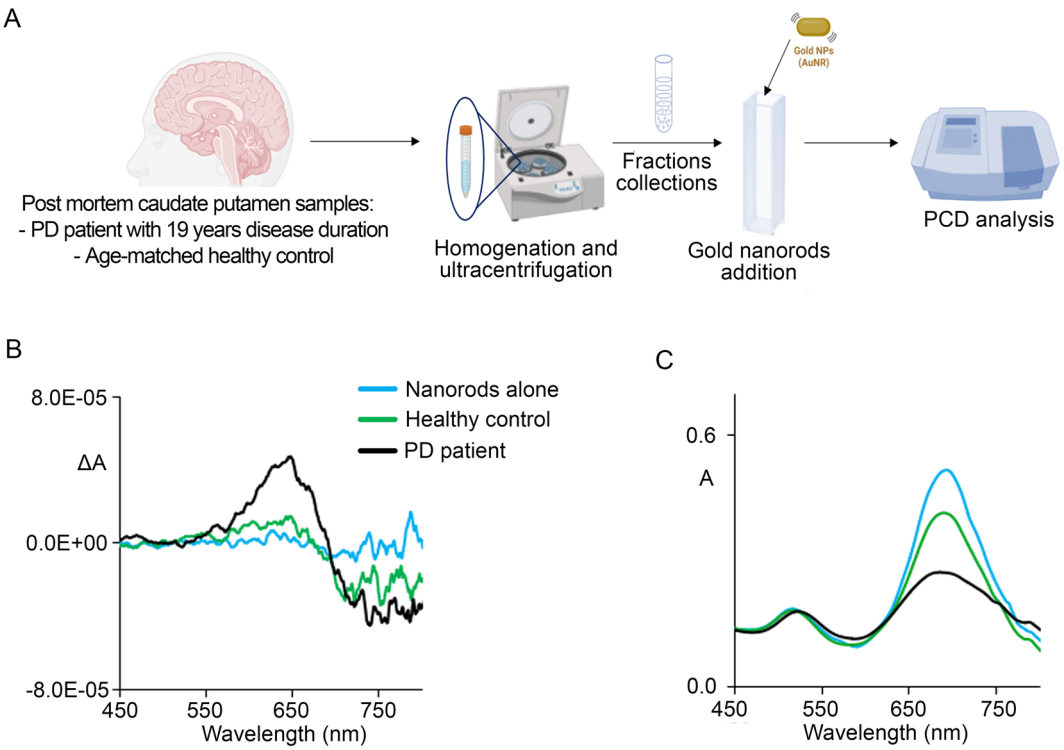

Fig. 2 (A) Schematic representation of the experimental design. (B) CD and (C) absorption spectra of nanorod suspensions (nanorod size: 10 × 30 nm) incubated for 1 h with purified human brain homogenate (black line) and healthy controls (green lines), compared with nanorods alone (blue line).

presence of αSyn fibrils from biological samples by nanorod-based PCD. Moreover, the broadening of the longitudinal surface band suggests that nanorod-based PCD may sense fibrils of different compositions, although the main positive peak centred at 650 nm supports that the main αSyn fibrillary species should be composed of fl αSyn.

Detection of fibrils from neuroblastoma cells

Subsequently, we performed nanorod-based PCD studies on fibrils derived from sucrose gradient-based fractionation of human SK-N-SH neuroblastoma cell clones stably overexpressing either human fl or Ctt αSyn of 120 amino acids in length, named SK140 and SK120, respectively. The control SK-N-SH cells, which only express endogenous fl αSyn (indicated as SK), were also analysed. In particular, we performed nanorod-based PCD analysis of the three lines either in basal condition or upon exposure to fl human αSyn monomers or sonicated PFF composed of either human fl or Ctt αSyn of 120 aa (1–120) (Fig. 3A) to disclose whether different exogenous fibrils can impact the morphology of endogenously generated fibrils.

Interestingly, we found that even the extracts from fractions 4–6 of the untreated control SK cells plated at a concentration of 80 000 cells per dish gave a bisignate CD signal when mixed with the nanorod suspension (Fig. 3B, green line). We also performed some tests to exclude optical artifacts. Although the preferential alignment of the fibrils within the cuvette is unlikely, we verified that the CD signal was independent of the orientation of the cuvette and that no linear dichroism could be detected by operating the photoelastic modulator at 100 kHz instead of 50 kHz, which is the standard modulation frequency for CD spectrometers (not shown).

Then, we repeated the nanorod-based PCD analysis on the extracts obtained starting from a lower cell amount (20 000 cells per dish) to check whether this diminished cell quantity could still allow the detection of a signal with a lower intensity. In particular, we added 100 μL of extract to the same quantity of nanorod suspension. Interestingly, we found that a lower cell number was associated with a lower PCD (Fig. S1A and B†).

We also performed culture extraction and PCD analysis using human embryonic kidney (HEK) cells plated at a concentration of 80 000 cells per dish as a negative control not presenting endogenous αSyn expression and we could not record PCD for the mixture of nanorods plus HEK fractions for up to 2 h of incubation at room temperature (Fig. S1C and D†). These results suggest that even the untreated SK-N-SH controls cells may contain a certain amount of fl αSyn protofibrils, which can be efficiently detected by nanorod-based PCD analysis, thus supporting the high sensitivity of this approach.

When we analysed and compared the sucrose gradient fractions 4–6 from the SK140, SK120 and SK cell extracts plated at a concentration of 80 000 cells per well, we could detect a (−,+) couplet from all the different samples. It is important to consider that while the CD signal intensity may be influenced by many factors including the single cell culture conditions, the wavelength shifts can be strictly dependent on the differences in fibril structures, which may impact the interaction and orientation of the nanorods, consequently affecting the CD signal. Notably, we observed a wavelength shift particularly evident in the positive, high-energy component of the CD couplet associated with the longitudinal plasmonic band of SK120 compared to both the SK140 and SK cell samples (Fig. 3B). Indeed, the CD signal from the SK120 samples was blue shifted with respect to that of the SK140 and SK samples. In particular, we found that the shift followed the order of $\lambda(\mathrm{SK120}) < \lambda(\mathrm{SK140}) \approx \lambda(\mathrm{SK})$. This suggests that the slightly different morphologies of the fl and 120 aa Ctt αSyn fibrils likely impacts the plasmonic nanorod response (Fig. 3B). Consistently, previous studies reported that the longitudinal bands of nanorod-based PCD spectra may be perturbed even by slight environmental changes such as dielectric constant variations.[48–50] Recently, more cogent considerations on the dependence of PCD signals on environmental conditions has been proposed in an experiment similar that herein conducted.[50] In addition, treatment based on exciton coupling[51] in a dimer nanorod model enabled the evaluation of the spectral position and shape of the longitudinal localized surface plasmon resonance.[52,53] More precise treatment of CD from the self-assembly of nanoparticles into optically active materials can be found in ref. 54 and 55, also accounting for plasmons coupled with semiconductor emitters. In any case, more sophisticated treatments also considering the electromagnetic field should be further explored,[56–58] but that is beyond the scope of this research.

Considering that PCD shifts could allow to distinguish the differences in the fibril conformations of fl and Ctt αSyn to be distinguished, we also analysed the normalized PCD spectra of SK140, SK120 and control SK cells exposed to fl human αSyn monomers (Fig. 3C) or human αSyn sonicated fl or Ctt (1–120) PFF (Fig. 3D and E). The treatment of SK140, SK120 or control SK cells with either αSyn monomers or sonicated fl or Ctt (1–120) αSyn PFF did not induce wavelength shifts in the spectrum with respect to that observed with the untreated cells, with the exception of the SK cells exposed to Ctt (1–120) αSyn sonicated PFF, which displayed a blue shift with a positive peak centred at the wavelength of SK120, as also evidenced in the non-normalized spectra (Fig. S2†). All the SK120 samples incubated with monomeric, fl or Ctt (1–120) αSyn produced a blue-shifted PCD, with the positive peak at the same wavelength for all treatments. Similar observations were derived from the analysis of all the SK140 samples. Therefore, assuming that nanorod-based PCD can distinguish the fl and Ctt (1–120) αSyn fibrils, our results support that the induced CD response from SK140 and SK120 is the one determined by the fibrils generated by the αSyn originally expressed by the cells and not by the PFF added to the cell culture. SK120 gave the same doublet, shifted with respect to SK140, regardless of the addition of fl or Ctt (1–120) αSyn PFF. Nevertheless, the addition of Ctt (1–120) αSyn sonicated PFF to the SK cell culture resulted in a blue shift in the CD signal compared to that we previously observed for the untreated control SK cells (Fig. 3B and E). These findings support that the PCD signal

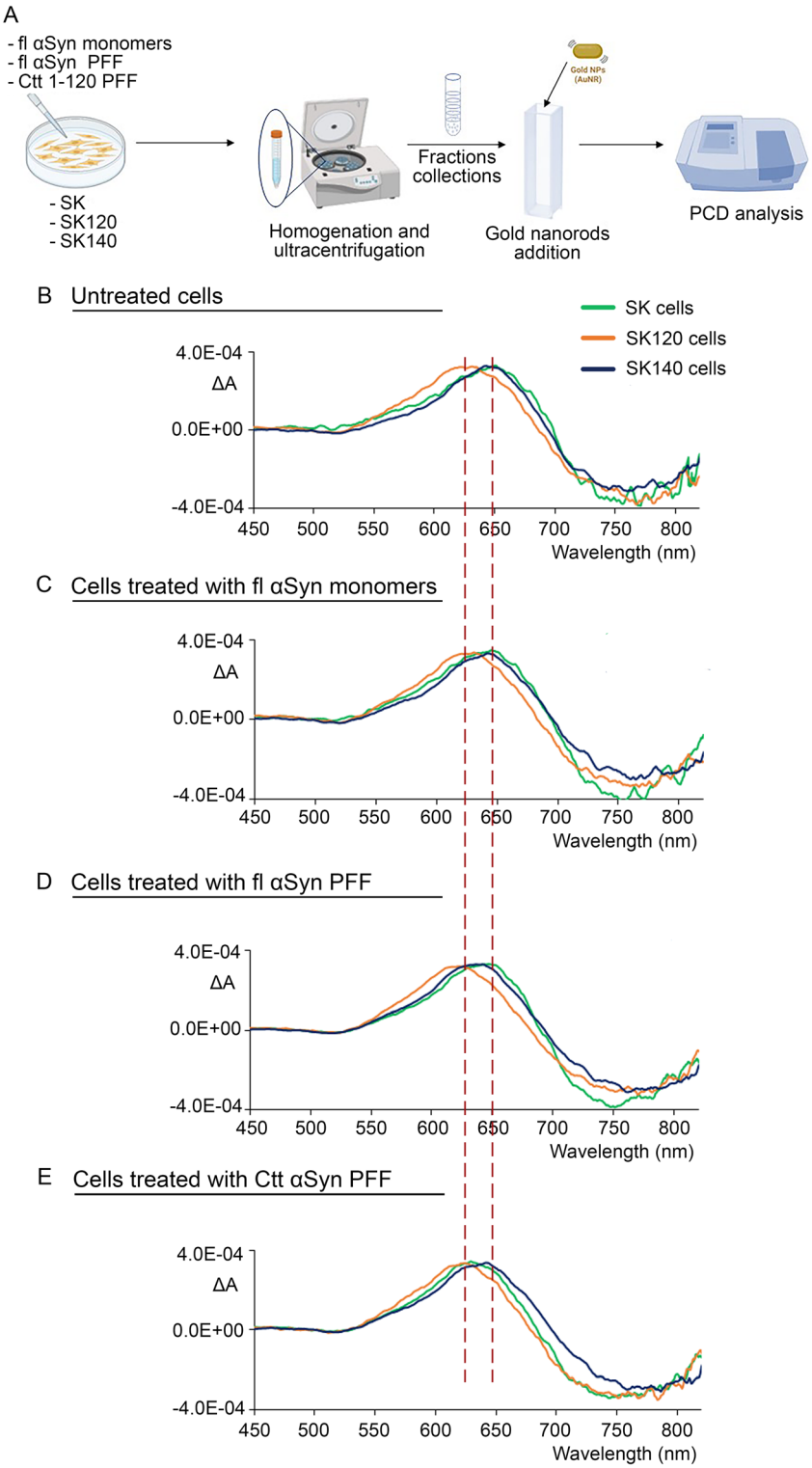

Fig. 3 (A) Schematic representation of the experimental design. Comparison of CD spectra of (10 × 30 nm) nanorod suspension incubated for 1 h with purified extracts from SK (green line), SK120 (orange line) and SK140 (blue line). (B) Untreated cells, (C) cells treated with fl αSyn monomers, (D) cells treated with fl αSyn PFF, and (E) cells treated with Ctt (1–120) αSyn PFF. All CD spectra have been normalized to facilitate comparison.

from the SK cells is likely derived from the protofibrils whose structure can still be affected by the addition of Ctt (1–120) PFF. Conversely, the signal collected from SK120 and SK140 was likely derived from more mature fibril structures that could not be perturbed by the further addition of fl or Ctt (1–120) PFF. These findings support that Ctt (1–120) αSyn PFF

can display a higher seeding-like activity on immature endogenous αSyn protofibrils but does not affect the structure of mature αSyn fibrils.

Detection of synthetic human fl or 1–120 aa Ctt αSyn fibrils

The wavelength shift observed in the main PCD peak between SK120 and SK140 suggested that it was worth further pursuing the spectroscopic study of this aspect. Given that Ctt αSyn is composed the core of LB and exhibits higher seeding ability compared to fl αSyn,[6,7,59] we performed nanorod-based PCD analysis of the human αSyn PFF generated *in vitro* from human fl and Ctt (1–120) αSyn or human fl αSyn monomers as a negative control (Fig. 4A). Indeed, although the PCD analysis of synthetic human fl αSyn PFF was already described by Kumar and co-authors,[31] they did not perform Ctt αSyn analysis.

Given that the use of synthetic PFF offered the possibility to work with different known concentrations, we first performed a sensitivity test with fl αSyn PFF starting from 0.1 nM suspensions to determine the limit of detection (Fig. S3†). We found that the CD couplet started to appear at a concentration of 0.5 nM (Fig. S3,† blue line). However, this signal was very weak and noisy. Thus, to avoid noisy spectra, while better evidencing the differences between fl and Ctt (1–120) αSyn, we decided to use higher concentrations for the subsequent tests.

The addition of 375 nM fl or Ctt (1–120) αSyn PFF to the nanorod solution generated an intense bisignate CD signal that was almost perfectly symmetric (Fig. 4B and D). The absorption spectra resulted in a decrease in intensity, a slight red shift and bandwidth increase in the longitudinal plasmon band (Fig. 4C and E). No CD was observed after incubating fl and Ctt (1–120) αSyn monomers at the same concentration with nanorods for up to 4 h of incubation (Fig. 4B and D inset), an observation corroborating that only fibrils serve as the chiral template for the nanorods.

Also, we observed that significant spectroscopic changes occurred roughly immediately after the addition of fl αSyn PFF, while in the case of Ctt (1–120) αSyn, about two hours were necessary to reach the final maximum CD intensity. The longer time needed to form the nanorod-Ctt (1–120) αSyn fibril complexes further suggests that there are key structural differences in the two types of fibrils, in agreement with the findings supporting that Ctt αSyn can fibrillate faster and generates fibrils that are different from the fl form.[10,60] Moreover, the cryo electron microscopy (EM) studies showed that Ctt αSyn of 121 amino acids in length forms fibril structures that differ from those formed from fl αSyn.[61] Our findings support that nanorods need more time to form a stable interaction with the Ctt αSyn fibrils, possibly also suggesting that they display a different helical rise and shift compared to the fl αSyn fibrils.

By superimposing the two PCD responses from the nanorods bound to the fl or Ctt PFF (Fig. 4F), we again detected a 14 nm wavelength blue shift in the Ctt (1–120) αSyn CD spectra with respect to that of fl αSyn. This wavelength shift is readable considering both the lower wavelength band of the couplet (less noisy) and the zero-crossing point of the CD doublet. It is worthwhile to stress that the spectral shift was obtained on the same batch of nanorods, with the same concentration, the same buffer for dilution, and the same instrumental set-up. The real reason for the shift is difficult to justify (different density while adsorbing on fibrils, different average orientation, and polydispersity of fibrils) but it turns out to be a useful parameter to distinguish fl from Ctt fibrils.

To further confirm the occurrence of the wavelength shift derived from the analysis of fl or Ctt αSyn PFF, we tested, under the same conditions, a different batch of 10 × 25 nm nanorods. Again, we observed a shift that was only slightly different for the two components of the doublet (Fig. S4†). Thus, this wavelength shift is reproducible *in vitro* and *in vivo* and it allows the discrimination of fl from Ctt αSyn fibrils.

Importantly, another relevant finding of this study is related to the fact that when comparing the analysis of the *in vitro* and *in vivo* samples, all the signals generated from the nanorods with fibrils extracted from AAV-hαSyn-injected mouse brains or from neuroblastoma cells consist of a CD couplet of reversed sign ("negative couplet") with respect to that obtained from the synthetic αSyn PFF ("positive couplet"),[51] which is consistent with previous studies.[31] Although the limited accessible spectroscopic range and the broadness of the signals may pose some doubts about the couplet definition, the results from the test with the 10 × 25 nm nanorod batch appear reliable, given that in this case, the couplet is far from the range limit (Fig. 5C). In addition, the difference between the signal of the *in vivo* and *in vitro* formed fibrils indicates that the arrangement of nanorods on *in vivo*-generated αSyn fibrils and PFF exhibits a different chirality. To further prove that the *in vivo* environment can influence the chirality of the fibrils, we incubated fl αSyn PFF (3.75 μM final concentration) with brain homogenate from αSyn null mice for 24 h, and then we added the 10 × 30 nm nanorod solution (Fig. 5A). We found that the signal obtained from this sample (Fig. 5D and E) was similar and had the same sign of that obtained from *in vivo* fibrils generated from the AAV-hαSyn-injected mice and SK140, and thus displayed the opposite sign compared to that obtained from the crude analysis of fl αSyn PFF (Fig. 5B and C).

This suggests that the *in vivo* environment may shape the fibrillation process and promote a different morphology, inducing the opposite chirality of the nanorods. On this line, recent studies reported different morphologies or handedness of brain-derived *vs. in vitro*-formed amyloid β fibrils.[62] In simple molecular systems, a CD symmetric couplet with alternating signs indicates their handedness, which may be proven by time-dependent density functional theory calculations[63] and simple coupled dipole models.[64] It has been shown that longitudinal plasmon oscillation is associated with a large electric dipole transition moment parallel to the nanorod long axis.[49] Thus, assuming the simple picture of interacting electric dipole transition moments, a (+,−) and (−,+) couplet (in order of decreasing wavelengths) may be related to opposite helix handedness. However, to draw a conclusion about right

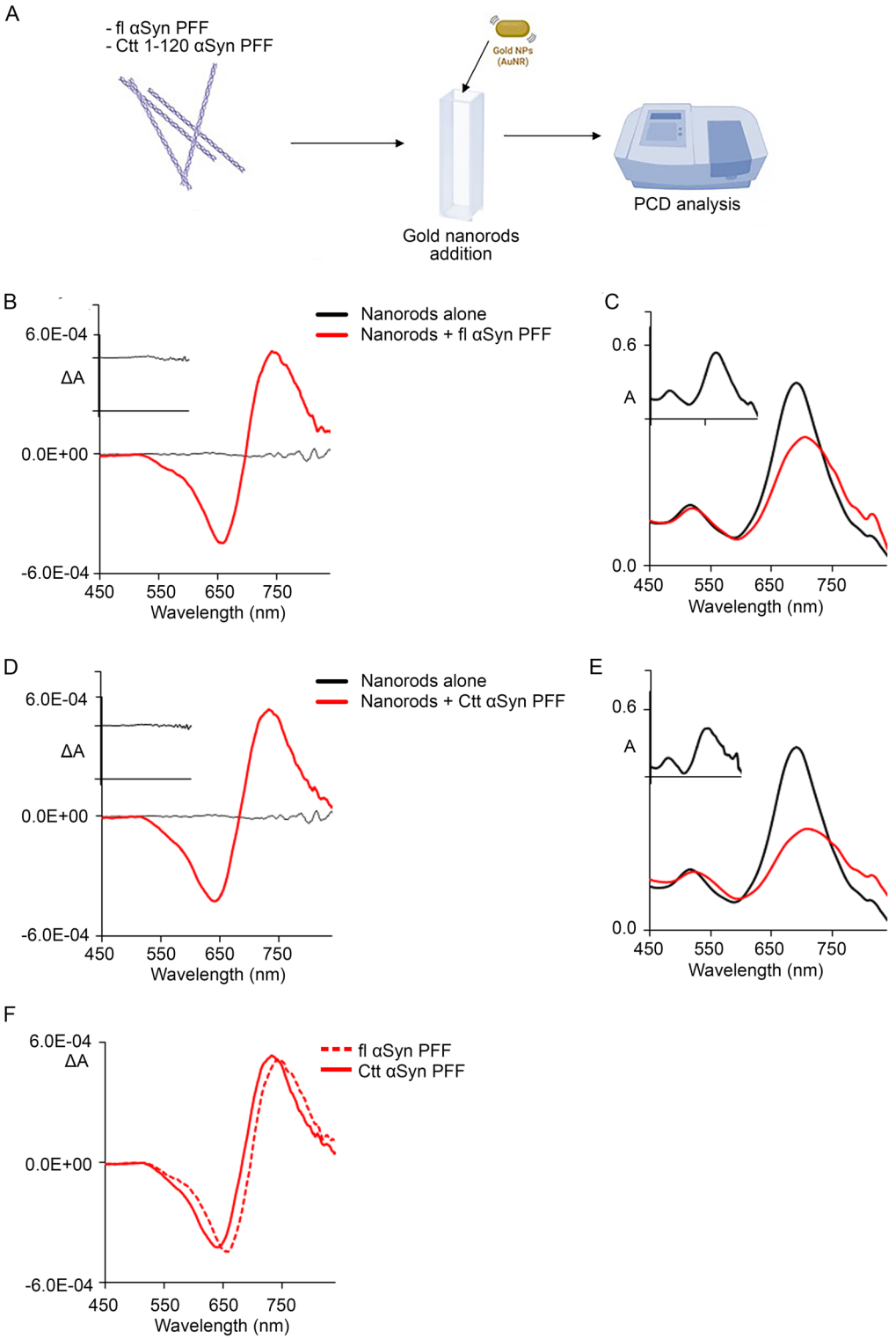

Fig. 4 (A) Schematic representation of the experimental design. (B) CD and (C) absorption spectra of (10 × 30 nm) nanorods for plain nanorod-buffer suspensions (black line) and for nanorod suspension mixed with 375 nM fl αSyn PFF (red line) incubated for 1 h. Spectra of fl αSyn monomers at the same concentration mixed with nanorods after 4 h of incubation in Inset. (D) CD and (E) absorption spectra of nanorods (10 × 30 nm) for plain buffer suspensions (black line) and after the addition of 375 nM Ctt (1–120) αSyn (red line) after 2 h of incubation. Spectra of Ctt monomers mixed with nanorods after 4 h of incubation in Inset. (F) Comparison of CD spectra of nanorod suspensions with fl αSyn (dash) and Ctt (1–120) PFF (solid).

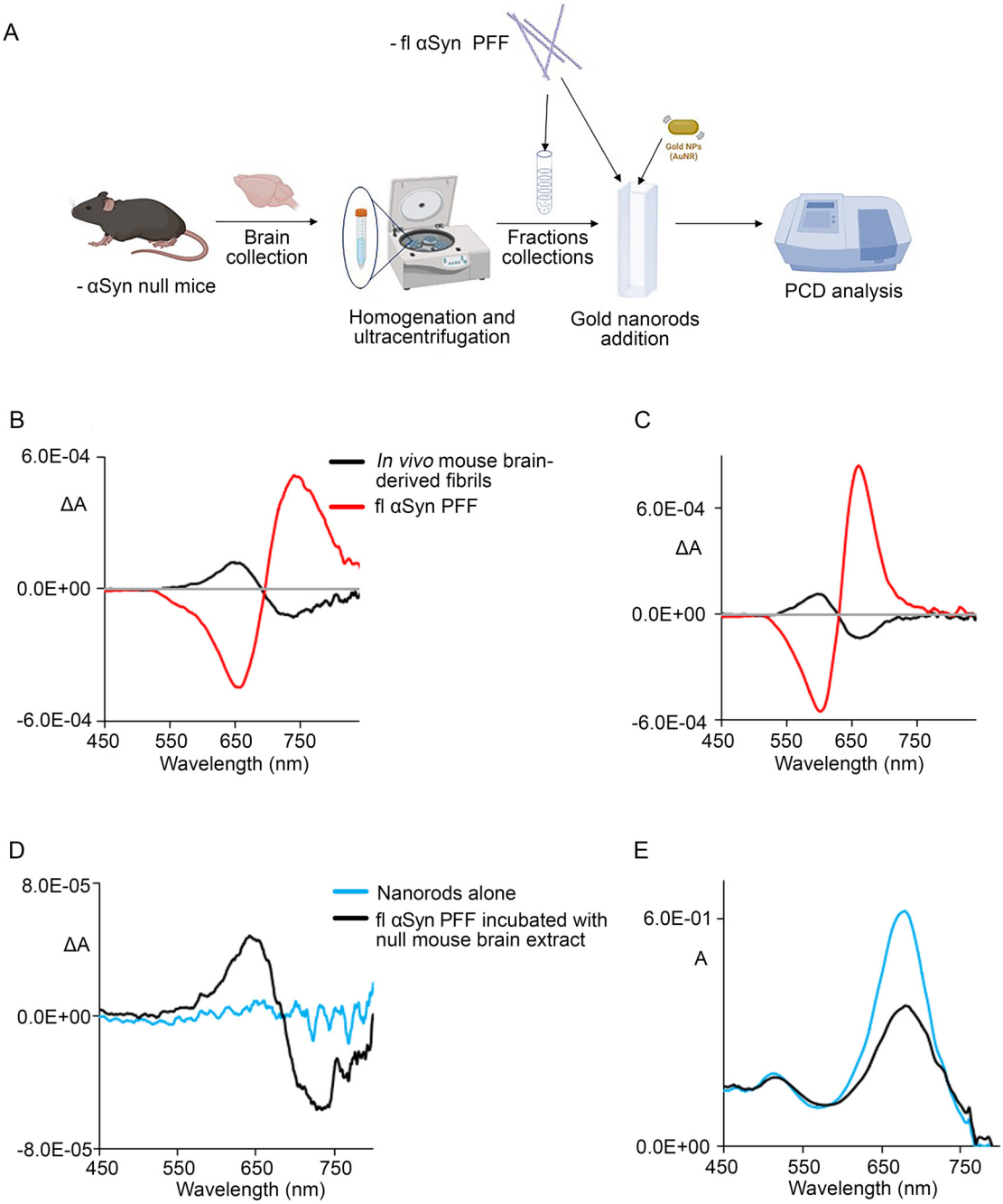

Fig. 5 (A) Schematic representation of the experimental design. CD spectra of 10 × 30 nm (B) and 10 × 25 nm and (C) nanorod suspensions incubated with fl αSyn PFF (red line) and with fibrils obtained from AAV-h αSyn-injected mouse brain homogenate (black line). (D) CD and (E) absorption spectra of nanorod suspensions incubated for 1 h with fl αSyn PFF+αSyn null mice brain tissue (24 h incubation). Nanorod size: 10 × 30 nm.

(*P*)- or left (*M*)-handed chirality, one should have specific information about the real geometrical arrangement of the electric dipole transition moments giving rise to an exciton couplet.[64] In particular, the "creeper" type and "helix" type geometries should be distinguished. A creeper assembly has longitudinally loosely arranged dipoles along a given axis (in our case the fibril axis), with the opposite CD couplet with respect to the case of the helix of the same handedness with dipoles transverse to the helix axis. Furthermore, other more sophisticated calculations accounting for electromagnetic interactions[23,57] should also be considered once a geometry is given.[31]

Nevertheless, to support the simple observations reported herein, it should also be considered that the influence of the environment on the fibril morphology (even handedness) is well known in the literature, and chiroptical spectroscopies have had a great part on these findings.[16–21]

In relation to the different chiroptical responses between the *in vivo* and *in vitro* systems, we found that the treatment of

SK140 or SK120 with PFF did not change the original (−,+) signal associated with the fibrils extracted under different conditions. In this regard, it has been observed that seeding experiments with brain filaments promote the fibrillation of recombinant human αSyn *in vitro* and generate assemblies different from that of the seeds.[65] In general, it is not easy *a priori* foresee how environmental factors influence the fibrillar evolution, and in this instance chiroptical spectroscopies may play an important role.[66]

In any case, it is quite noticeable that the reversal of the couplet sign comparing the *in vivo* and *in vitro* prepared samples does not affect the shift between the fl and Ctt forms.

TEM-based analysis of the nanorod-fibrils complexes

Given that our data support that nanorod-based PCD analysis allows the differentiation of fl and Ctt (1–120) fibrils and to distinguish the synthetic PFF from the fibrils generated *in vivo*, we used TEM to acquire some information about nanorods and PFF surface interaction. The images were recorded for nanorods mixed with fl and Ctt (1–120) αSyn PFF.

We observed that the nanorods cover most of the surface of the fl PFF (Fig. 6A). The presence of free nanorods in the analysed solution is consistent with the saturation of PFF binding. The analysis of the higher magnification images (Fig. 6B)

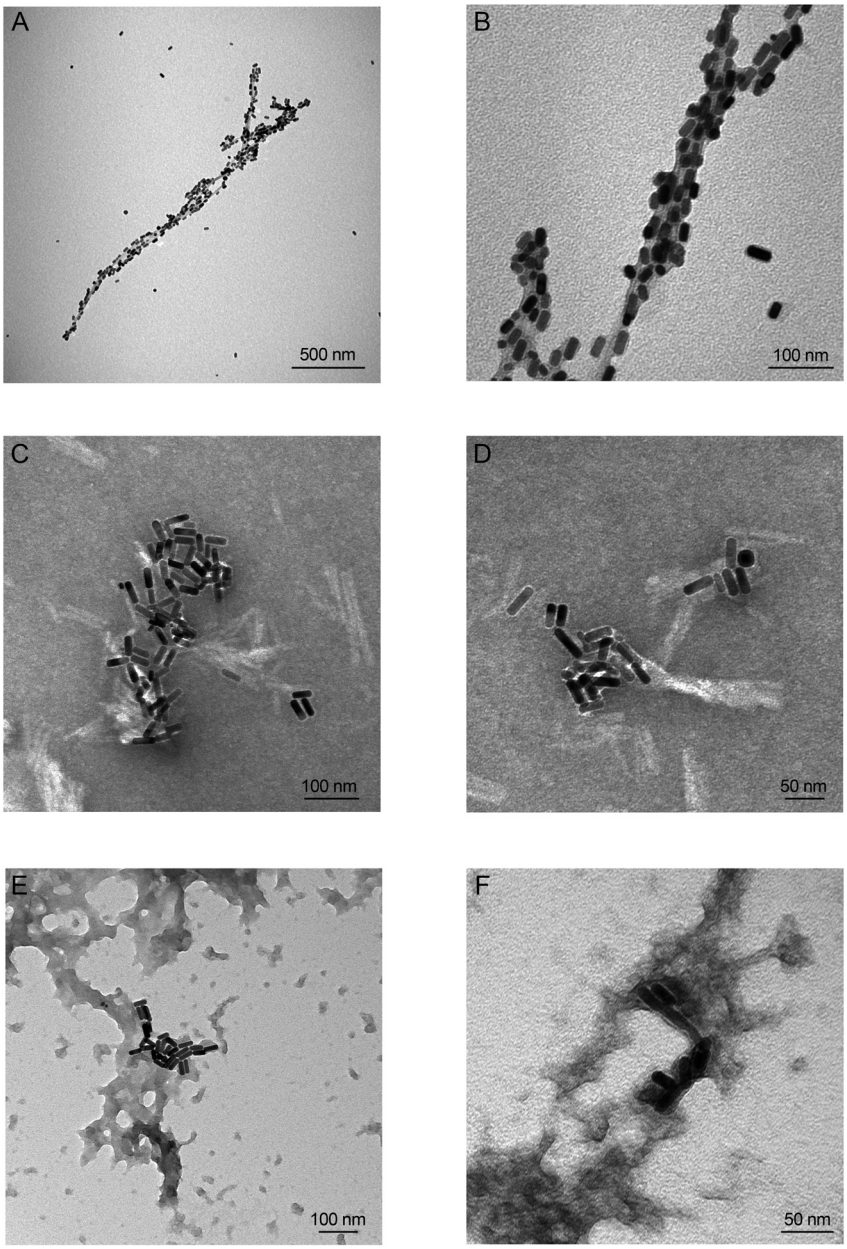

Fig. 6 TEM images of (A) fl αSyn PFF interacting with 10 × 25 nm nanorods, scale bar = 500 nm and (B) at high magnification, scale bar = 100 nm (B) and (C) Ctt (1–120) αSyn PFF interacting with 10 × 30 nm nanorods at scale bar = 100 nm and (D) scale bar = 50 nm. TEM images of (E) SK140 and of (F) SK120 neuroblastoma cell extracts at scale bar = 100 nm.

showed that the nanorods were arranged along the longitudinal axis of fl αSyn PFF, mostly parallel to the direction of fibril, similar to a "creeper" arrangement.[64]

Alternatively, the TEM images of the complex nanorods-Ctt (1–120) PFF (Fig. 6C and D) showed that these fibrils form assemblies, inducing the interaction with nanorods with a mixed orientation (parallel or transverse with respect to the fibril axis) only in some of their portions. Both the Ctt (1–120) αSyn and nanorod arrangement appeared disordered in this case.

Similarly, the TEM images of the fibrils purified from SK 140 (Fig. 5E) and SK120 (Fig. 5F) mixed with nanorods showed the presence of fibril clumps. Again, the nanorods were found to be attached to some parts of the fibrils in mixed directions.

These findings support the idea that the wavelength shift observed between the synthetic or biological fl and Ctt fibrils cannot be easily correlated with the nanorod orientation and that other techniques such as cryo-EM, which can also detect the direction of handedness, should be undertaken to explain this correlation. In any case, it clearly appears that the chiral partial ordering onto nanorods is imparted by the fibrils.

Right- or left-handed fibrils?

In the last few years, cryo-electron microscopy (cryo-EM) studies disclosed the morphology of human brain-derived and synthetic αSyn fibrils. Synthetic and post-mortem brain-derived fibrils from MSA patients have been found to display left-handed twist.[15,31,61,67–70] However, the fibrils purified from the post-mortem brains of PD and DLB patients were shown to exhibit a right-handed twist.[71] Given that we observed that the αSyn fibrils generated *in vitro* and *in vivo* show reverse PCD spectra, possibly suggesting their opposite chirality, we decided to also run PCD experiments with insulin fibrils prepared by well-established protocols, allowing the generation of fibrils with the opposite chiroptical response.[17,19,21,72]

In the case of insulin fibrils, previous VCD studies have detected sign changes when the fibrils were produced under different conditions.[21,72] Analogously, it has been demonstrated that insulin fibrillation and chirality can be assessed by recording induced CD and CPL on achiral thioflavinT (ThT).[19] The incubation of nanorods with the two types of insulin fibrils prepared as we previously described[19] also showed a very intense PCD signal with a slightly asymmetric couplet (+,−) or (−,+) (Fig. 7). This supports that the nanorods assemble in the opposite way in the presence of the two types of insulin fibrils.

Based on this, given that our data show opposite couplets for the *in vivo* and *in vitro*-generated αSyn fibrils and considering the cryo-TEM studies,[69,71] it may be feasible that the (−,+) couplet (in order of increasing wavelength) observed for PFF reflects their left creeper-handedness. Conversely, the (+,−) couplet recorded for *in vivo*-generated fibrils would likely reflect their right creeper-handedness. In this line, the (+,−) couplet obtained from the PCD of PFF incubated with αSyn null mouse brain extracts could indicate PFF handedness inversion upon incubation with biological material. Findings indicating that incubation conditions (presence of lipids, other proteins, and different pH or salt concentrations) affect the PFF shape and handedness[73] further support that the observed sign change in the PFF nanorod-based PCD upon incubation in the biological environment may reflect handedness reversal.

It is also worth considering that other chiroptical spectroscopies have been used to study the morphology and handedness of a specific truncated form of αSyn (1–108 aa)[15] or the contribution of lipids to the fibrillation of the 71–82 aa αSyn peptide, known as the fibrillation-prone core of the non-amyloid component domain of αSyn.[22] In particular, Martial *et al.*[22] assigned opposite VCD couplets observed in different conditions to either left-twisted fibrils or right-twisted fibrils, further supporting our hypothesis.

All things considered, our findings indicate that nanorod-based PCD can be used to detect defined senses of handedness and can represent a helpful tool to study the fibril mor-

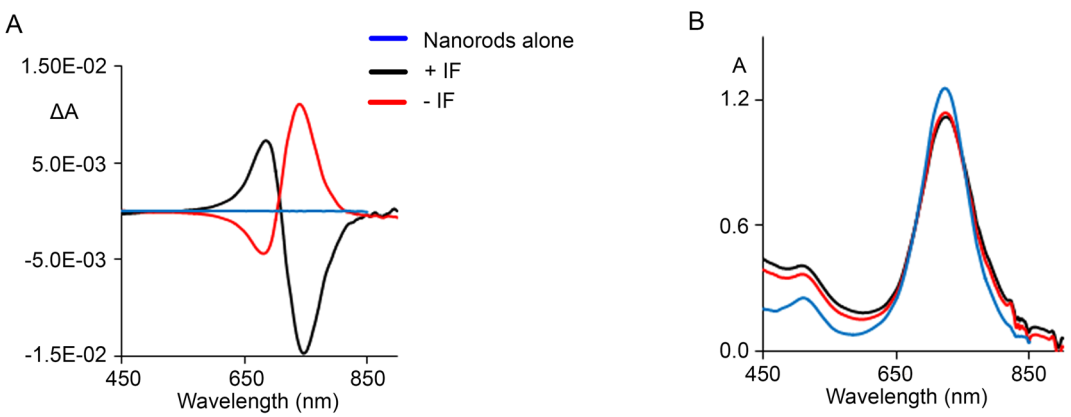

Fig. 7 (A) CD spectra of nanorod solutions (10 × 30 nm) incubated for 1 h with +insulin fibrils (+IF) (red line) and −insulin fibrils (−IF) (black line). (B) Nanorod absorption spectra for + IF and −IF. Nanorod solution spectra without fibrils is also shown (blue line). Please note that, after ThT staining, +IF and −IF gave positive and negative CD, respectively.

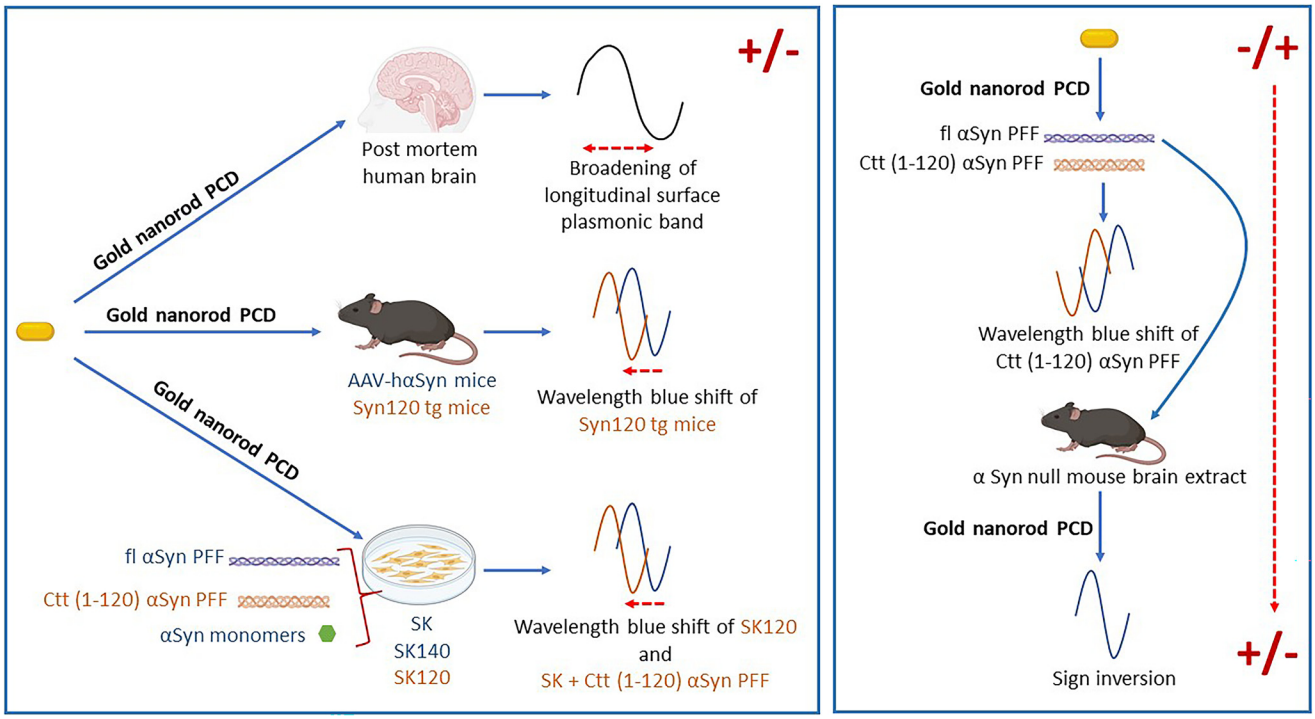

Fig. 8 Schematic representation of the results of this study.

phology and follow the changes in the structure and morphology of αSyn fibrils during fibrillation.

Conclusions

This study demonstrated that the PCD signals from nanorods incubated with αSyn fibrils consist of a nearly symmetric bisignate couplet centred corresponding to the absorption maximum and are highly reproducible across different samples of biological origin.

As summarized in Fig. 8, independent of the fibril origin (generated *in vitro* or purified from biological material), a blue wavelength shift in the main CD peak characterizes Ctt αSyn plus nanorod – compared to the fl αSyn plus nanorod-derived couplets. Strikingly, the CD measurements showed sign inversion between PFF generated from the recombinant αSyn and the αSyn fibrils purified from biological material, suggesting opposite handedness in the fibril morphology. Nevertheless, we found that the exposure of PFF to a biological environment led to a CD couplet inversion supporting handedness inversion. Finally, we also found that the addition of fl (or Ctt) αSyn PFF to cells overexpressing fl or Ctt αSyn did not affect the CD signal, indicating that mature fibrils cannot be shaped by the addition of different exogenous PFF. Nevertheless, the incubation of SK cells with Ctt (1–120) PFF produced a blue wavelength shift, supporting the fact that exogenous Ctt fibrils can shape the intracellular fl αSyn protofibril morphology. Collectively, these findings support the fact that the nanorod-based PCD generated from αSyn fibrils constitutes a valid tool to gain significant insights into the complexity of αSyn aggregates in synucleinopathies. It reliably distinguished the fibrils generated from fl and Ctt αSyn, and also disclosed that the structure of mature intracellularly generated fibrils is not influenced by exposure to exogenous αSyn, while smaller intracellular fl αSyn aggregates are still susceptible to conformational changes and can be affected by the fibrils formed by Ctt αSyn, which being abundant in the core of LB, can constitute the first nucleation sites for αSyn aggregation. This supports that the chiroptical technique adopted herein is capable of detecting nanomolar quantities of homogenates of biological tissues, which can provide relevant information for the characterization of fibrils from biological samples.

Author contributions

FL: Methodology, formal analysis, investigation, validation, writing – original draft, writing – review and editing; RB: methodology, formal analysis, investigation, validation, writing – original draft; VB: formal analysis; MS: methodology, formal analysis, investigation; LB: resources, supervision, writing – review and editing; SA: conceptualization, methodology, resources, funding acquisition, project administration, supervision, writing – original draft, writing – review and editing; GL: conceptualization, methodology, formal analysis, investigation, validation, resources, funding acquisition, project administration, data curation, supervision, writing – original draft, writing – review and editing; AB: conceptualization, methodology, resources, data curation, funding acquisition,

project administration, supervision, writing – original draft, writing – review and editing.

Data availability

Data for this article are deposited at a personal repository and will be available from the authors. URL and access will be provided upon request.

The ESI,† available free of charge, contains further chiroptical data recalled in the text.

Conflicts of interest

The authors declare that they have no conflict of interest.

Acknowledgements

RB, GL and SA thank the PhD school "Molecular Genetics, Biotechnologies and Experimental Medicine" in the University of Brescia, for supporting RB throughout her PhD studies. The Italian Ministry of University and Research (PRIN 2017 program 2017A4XRCA_003) is acknowledged for funding. AB is grateful to the Michael J. Fox Foundation for Parkinson's disease, NY, USA (Target Advancement Program, grant ID #10742.01) and to the Italian MIUR PRIN 2017-1065.

References

1 C. A. Ross and M. A. Poirier, *Nat. Med.*, 2004, **10**(Suppl), S10–S17.
2 M. G. Spillantini, R. A. Crowther, R. Jakes, M. Hasegawa and M. Goedert, *Proc. Natl. Acad. Sci. U. S. A.*, 1998, **95**, 6469–6473.
3 M. G. Spillantini and M. Goedert, *Cell Tissue Res.*, 2018, **373**, 137–148.
4 A. Bellucci, N. B. Mercuri, A. Venneri, G. Faustini, F. Longhena, M. Pizzi, C. Missale and P. Spano, *Neuropathol. Appl. Neurobiol.*, 2016, **42**, 77–94.
5 M. Baba, S. Nakajo, P. H. Tu, T. Tomita, K. Nakaya, V. M. Lee, J. Q. Trojanowski and T. Iwatsubo, *Am. J. Pathol.*, 1998, **152**, 879–884.
6 R. A. Crowther, R. Jakes, M. G. Spillantini and M. Goedert, *FEBS Lett.*, 1998, **436**, 309–312.
7 K. Prasad, T. G. Beach, J. Hedreen and E. K. Richfield, *Brain Pathol.*, 2012, **22**, 811–825.
8 Z. A. Sorrentino, N. Vijayaraghavan, K. M. Gorion, C. J. Riffe, K. H. Strang, J. Caldwell and B. I. Giasson, *J. Biol. Chem.*, 2018, **293**, 18914–18932.
9 S. Huang, X. Mo, J. Wang, X. Ye, H. Yu and Y. Liu, *FEBS Lett.*, 2022, **596**, 1388–1400.
10 X. Ni, R. P. McGlinchey, J. Jiang and J. C. Lee, *J. Mol. Biol.*, 2019, **431**, 3913–3919.
11 P. Ruzza, R. Hussain, B. Biondi, A. Calderan, I. Tessari, L. Bubacco and G. Siligardi, *Biomolecules*, 2015, **5**, 724–734.
12 B. C. Jung, Y. J. Lim, E. J. Bae, J. S. Lee, M. S. Choi, M. K. Lee, H. J. Lee, Y. S. Kim and S. J. Lee, *Exp. Mol. Med.*, 2017, **49**, e314.
13 C. D. Syme, E. W. Blanch, C. Holt, R. Jakes, M. Goedert, L. Hecht and L. D. Barron, *Eur. J. Biochem.*, 2002, **269**, 148–156.
14 A. Kurochka, J. Prusa, J. Kessler, J. Kapitan and P. Bour, *Phys. Chem. Chem. Phys.*, 2021, **23**, 16635–16645.
15 A. Iyer, S. J. Roeters, V. Kogan, S. Woutersen, M. Claessens and V. Subramaniam, *J. Am. Chem. Soc.*, 2017, **139**, 15392–15400.
16 E. Van de Vondel, P. Baatsen, R. Van Elzen, A. M. Lambeir, T. A. Keiderling, W. A. Herrebout and C. Johannessen, *Biochemistry*, 2018, **57**, 5989–5995.
17 A. Loksztejn and W. Dzwolak, *J. Mol. Biol.*, 2008, **379**, 9–16.
18 R. Dec, V. Babenko and W. Dzwolak, *RCS Adv.*, 2016, **6**, 97331–97337.
19 A. Rybicka, G. Longhi, E. Castiglioni, S. Abbate, W. Dzwolak, V. Babenko and M. Pecul, *ChemPhysChem*, 2016, **17**, 2931–2937.
20 M. Krupova, J. Kapitan and P. Bour, *ACS Omega*, 2019, **4**, 1265–1271.
21 D. Kurouski, R. K. Dukor, X. Lu, L. A. Nafie and I. K. Lednev, *Biophys. J.*, 2012, **103**, 522–531.
22 B. Martial, T. Lefevre, T. Buffeteau and M. Auger, *ACS Nano*, 2019, **13**, 3232–3242.
23 D. Vila-Liarte, N. A. Kotov and L. M. Liz-Marzan, *Chem. Sci.*, 2022, **13**, 595–610.
24 G. Zheng, J. He, V. Kumar, S. Wang, I. Pastoriza-Santos, J. Perez-Juste, L. M. Liz-Marzan and K. Y. Wong, *Chem. Soc. Rev.*, 2021, **50**, 3738–3754.
25 F. Lu, Y. Tian, M. Liu, D. Su, H. Zhang, A. O. Govorov and O. Gang, *Nano Lett.*, 2013, **13**, 3145–3151.
26 A. O. Govorov, Z. Fan, P. Hernandez, J. M. Slocik and R. R. Naik, *Nano Lett.*, 2010, **10**, 1374–1382.
27 J. M. Slocik, A. O. Govorov and R. R. Naik, *Nano Lett.*, 2011, **11**, 701–705.
28 Z. Li, Z. Zhu, W. Liu, Y. Zhou, B. Han, Y. Gao and Z. Tang, *J. Am. Chem. Soc.*, 2012, **134**, 3322–3325.
29 D. Liu, W. Li, X. Jiang, S. Bai, J. Liu, X. Liu, Y. Shi, Z. Kuai, W. Kong, R. Gao and Y. Shan, *Theranostics*, 2019, **9**, 2268–2281.
30 M. Li, Y. Guan, A. Zhao, J. Ren and X. Qu, *Theranostics*, 2017, **7**, 2996–3006.
31 J. Kumar, H. Erana, E. Lopez-Martinez, N. Claes, V. F. Martin, D. M. Solis, S. Bals, A. L. Cortajarena, J. Castilla and L. M. Liz-Marzan, *Proc. Natl. Acad. Sci. U. S. A.*, 2018, **115**, 3225–3230.
32 M. E. Stewart, C. R. Anderton, L. B. Thompson, J. Maria, S. K. Gray, J. A. Rogers and R. G. Nuzzo, *Chem. Rev.*, 2008, **108**, 494–521.
33 G. Faustini, F. Longhena, T. Varanita, L. Bubacco, M. Pizzi, C. Missale, F. Benfenati, A. Bjorklund, P. Spano and A. Bellucci, *Acta Neuropathol.*, 2018, **136**, 621–639.

34 A. R. Carta, L. Boi, A. Pisanu, M. F. Palmas, E. Carboni and A. De Simone, *J. Neurosci. Methods*, 2020, **338**, 108685.
35 G. Faustini, F. Longhena, A. Bruno, F. Bono, J. Grigoletto, L. La Via, A. Barbon, A. Casiraghi, V. Straniero, E. Valoti, G. Costantino, F. Benfenati, C. Missale, M. Pizzi, M. G. Spillantini and A. Bellucci, *Neurobiol. Dis.*, 2020, **138**, 104789.
36 P. Garcia-Reitbock, O. Anichtchik, A. Bellucci, M. Iovino, C. Ballini, E. Fineberg, B. Ghetti, L. Della Corte, P. Spano, G. K. Tofaris, M. Goedert and M. G. Spillantini, *Brain*, 2010, **133**, 2032–2044.
37 G. K. Tofaris, P. Garcia-Reitbock, T. Humby, S. L. Lambourne, M. O'Connell, B. Ghetti, H. Gossage, P. C. Emson, L. S. Wilkinson, M. Goedert and M. G. Spillantini, *J. Neurosci.*, 2006, **26**, 3942–3950.
38 C. G. Specht and R. Schoepfer, *BMC Neurosci.*, 2001, **2**, 11.
39 F. Longhena, G. Faustini, T. Varanita, M. Zaltieri, V. Porrini, I. Tessari, P. L. Poliani, C. Missale, B. Borroni, A. Padovani, L. Bubacco, M. Pizzi, P. Spano and A. Bellucci, *Brain Pathol.*, 2018, **28**, 875–888.
40 A. Recasens, I. Carballo-Carbajal, A. Parent, J. Bove, E. Gelpi, E. Tolosa and M. Vila, *Acta Neuropathol. Commun.*, 2018, **6**, 8.
41 P. K. Jain, K. S. Lee, I. H. El-Sayed and M. A. El-Sayed, *J. Phys. Chem. B*, 2006, **110**, 7238–7248.
42 L. Streubel-Gallasch, V. Giusti, M. Sandre, I. Tessari, N. Plotegher, E. Giusto, A. Masato, L. Iovino, I. Battisti, G. Arrigoni, D. Shimshek, E. Greggio, M. E. Tremblay, L. Bubacco, A. Erlandsson and L. Civiero, *Mol. Neurobiol.*, 2021, **58**, 3119–3140.
43 A. Mingione, F. Pivari, N. Plotegher, M. Dei Cas, A. Zulueta, T. Bocci, M. Trinchera, E. Albi, V. Maglione, A. Caretti, L. Bubacco, R. Paroni, D. Bottai, R. Ghidoni and P. Signorelli, *Int. J. Mol. Sci.*, 2021, **22**(12), 6469.
44 T. Ikenoue, Y. H. Lee, J. Kardos, M. Saiki, H. Yagi, Y. Kawata and Y. Goto, *Angew. Chem., Int. Ed.*, 2014, **53**, 7799–7804.
45 N. K. Polinski, L. A. Volpicelli-Daley, C. E. Sortwell, K. C. Luk, N. Cremades, L. M. Gottler, J. Froula, M. F. Duffy, V. M. Y. Lee, T. N. Martinez and K. D. Dave, *J. Parkinson's Dis.*, 2018, **8**, 303–322.
46 D. Emin, Y. P. Zhang, E. Lobanova, A. Miller, X. Li, Z. Xia, H. Dakin, D. I. Sideris, J. Y. L. Lam, R. T. Ranasinghe, A. Kouli, Y. Zhao, S. De, T. P. J. Knowles, M. Vendruscolo, F. S. Ruggeri, F. I. Aigbirhio, C. H. Williams-Gray and D. Klenerman, *Nat. Commun.*, 2022, **13**, 5512.
47 A. S. Buchman, L. Yu, R. S. Wilson, J. A. Schneider and D. A. Bennett, *Neurology*, 2013, **80**, 2055–2061.
48 K. L. Kelly, E. Coronado, L. L. Zhao and G. C. Schatz, *J. Phys. Chem.*, 2003, **107**, 668–677.
49 S. Link, M. B. Mohamed and M. A. El-Sayed, *J. Phys. Chem.*, 1999, **103**, 3073–3077.
50 J. Kumar, E. Lopez-Martinez, A. L. Cortajarena, D. M. Solis, J. M. Taboada, B. Díez-Buitrago, V. Pavlov and L. M. Liz-Marzán, *Part. Part. Syst. Charact.*, 2019, **36**(5), 1800368.
51 N. Harada and K. Nakanishi, *Acc. Chem. Res.*, 1972, **5**, 257–263.
52 B. Auguie, J. L. Alonso-Gomez, A. Guerrero-Martinez and L. M. Liz-Marzan, *J. Phys. Chem. Lett.*, 2011, **2**, 846–851.
53 N. S. S. Nizar, M. Sujith, K. Swathi, C. Sissa, A. Painelli and K. G. Thomas, *Chem. Soc. Rev.*, 2021, **50**, 11208–11226.
54 N. A. Kotov, *Science*, 2010, **330**, 188–189.
55 J. Lu, Y. Xue, K. Bernardino, N. N. Zhang, W. R. Gomes, N. S. Ramesar, S. Liu, Z. Hu, T. Sun, A. F. de Moura, N. A. Kotov and K. Liu, *Science*, 2021, **371**, 1368–1374.
56 H. Zhang and A. O. Govorov, *Phys. Rev. B*, 2013, **87**, 075410.
57 D. M. Solis, J. M. Taboada, F. Obelleiro, L. M. Liz-Marzan and F. J. Garcia de Abajo, *ACS Nano*, 2014, **8**, 7559–7570.
58 M. Obelleiro-Liz, V. F. Martín, D. M. Solis, J. M. Taboada, F. Obelleiro and L. M. Liz-Marzán, *Adv. Opt. Mater.*, 2023, **11**(18), 2203090.
59 A. W. Michell, G. K. Tofaris, H. Gossage, P. Tyers, M. G. Spillantini and R. A. Barker, *Cell Transplant.*, 2007, **16**, 461–474.
60 U. Cendrowska, P. J. Silva, N. Ait-Bouziad, M. Muller, Z. P. Guven, S. Vieweg, A. Chiki, L. Radamaker, S. T. Kumar, M. Fandrich, F. Tavanti, M. C. Menziani, A. Alexander-Katz, F. Stellacci and H. A. Lashuel, *Proc. Natl. Acad. Sci. U. S. A.*, 2020, **117**, 6866–6874.
61 R. Guerrero-Ferreira, L. Kovacik, D. Ni and H. Stahlberg, *Curr. Opin. Neurobiol.*, 2020, **61**, 89–95.
62 M. Kollmer, W. Close, L. Funk, J. Rasmussen, A. Bsoul, A. Schierhorn, M. Schmidt, C. J. Sigurdson, M. Jucker and M. Fandrich, *Nat. Commun.*, 2019, **10**, 4760.
63 H. Xiang, Z. Wang, L. Xu, X. Zhang and G. Lu, *J. Phys. Chem.*, 2019, **124**, 945–951.
64 K. Swathi, C. Sissa, A. Painelli and K. George Thomas, *Chem. Commun.*, 2020, **56**, 8281–8284.
65 S. Lovestam, M. Schweighauser, T. Matsubara, S. Murayama, T. Tomita, T. Ando, K. Hasegawa, M. Yoshida, A. Tarutani, M. Hasegawa, M. Goedert and S. H. W. Scheres, *FEBS Open Bio*, 2021, **11**, 999–1013.
66 N. Hachlica, A. Kolodziejczyk, M. Rawski, M. Gorecki, A. Wajda and A. Kaczor, *Spectrochim. Acta, Part A*, 2024, **304**, 123293.
67 R. Guerrero-Ferreira, N. M. Taylor, A. A. Arteni, P. Kumari, D. Mona, P. Ringler, M. Britschgi, M. E. Lauer, A. Makky, J. Verasdonck, R. Riek, R. Melki, B. H. Meier, A. Bockmann, L. Bousset and H. Stahlberg, *eLife*, 2019, **8**, e48907.
68 R. Guerrero-Ferreira, N. M. Taylor, D. Mona, P. Ringler, M. E. Lauer, R. Riek, M. Britschgi and H. Stahlberg, *eLife*, 2018, **7**, e36402.
69 M. Schweighauser, Y. Shi, A. Tarutani, F. Kametani, A. G. Murzin, B. Ghetti, T. Matsubara, T. Tomita, T. Ando, K. Hasegawa, S. Murayama, M. Yoshida, M. Hasegawa, S. H. W. Scheres and M. Goedert, *Nature*, 2020, **585**, 464–469.
70 Y. Li, C. Zhao, F. Luo, Z. Liu, X. Gui, Z. Luo, X. Zhang, D. Li, C. Liu and X. Li, *Cell Res.*, 2018, **28**, 897–903.

71 Y. Yang, Y. Shi, M. Schweighauser, X. Zhang, A. Kotecha, A. G. Murzin, H. J. Garringer, P. W. Cullinane, Y. Saito, T. Foroud, T. T. Warner, K. Hasegawa, R. Vidal, S. Murayama, T. Revesz, B. Ghetti, M. Hasegawa, T. Lashley, S. H. W. Scheres and M. Goedert, *Nature*, 2022, **610**, 791–795.
72 S. Ma, X. Cao, M. Mak, A. Sadik, C. Walkner, T. B. Freedman, I. K. Lednev, R. K. Dukor and L. A. Nafie, *J. Am. Chem. Soc.*, 2007, **129**, 12364–12365.
73 W. Hoyer, T. Antony, D. Cherny, G. Heim, T. M. Jovin and V. Subramaniam, *J. Mol. Biol.*, 2002, **322**, 383–393.